

Robust Physical Hard-Label Attacks on Deep Learning Visual Classification

Ryan Feng^{*}, Jiefeng Chen[†], Nelson Manohar^{*}, Earlence Fernandes[†], Somesh Jha[†], Atul Prakash^{*}

^{*}University of Michigan, Ann Arbor, [†]University of Wisconsin, Madison

^{*}{rtfeng, nelsonr, aprakash}@umich.edu, [†]{jiefeng, earlence, jha}@cs.wisc.edu

Abstract—Existing automated attack-generation algorithms for machine learning models for computer vision tend to focus on digital attacks within an ϵ -ball around the input in white-box and black-box settings. However, in the real world, a more interesting class of attacks are those that are physically-realizable – say, by placing unobtrusive stickers on a traffic sign to cause a change in its classification. Given a model, generating such attacks automatically is still a challenge, even in white-box settings. We present GRAPHITE, an algorithm to automatically find small areas to place robust adversarial perturbations in the black-box *hard-label* setting where the attacker only has access to the model prediction class label. Unlike algorithms for digital attacks that only aim to minimize perturbation based on an L_p norm (typically L_2 or L_∞), the proposed algorithm automatically generates robust adversarial examples that (1) have a high success rate under multiple transformations that simulate, for example, viewing point changes and (2) occupy a small area on the image so that they are more likely to be physically realizable as stickers. Using GRAPHITE, we successfully attack a stop sign to be misclassified as a speed limit 30 km/hr sign in 92.86% of physical test images with fewer than 124k queries.

I. INTRODUCTION

Machine learning (ML) models, such as deep-neural networks (DNNs), have had resounding success in several scenarios such as face and object recognition [1], [2], [3], [4], [5]. However, researchers have discovered that these ML models are vulnerable to several adversarial attacks, such as test-time, training-time, and backdoor attacks [6], [7], [8], [9], [10], [11]. For a comprehensive tutorial on adversarial ML readers should consult [12]. These attacks have raised concerns for deploying these models in critical settings, such as autonomous driving, security, and cyber-physical systems (CPSs).

In this paper we consider *physical* attacks in the black-box *hard-label* setting. These attacks fall under a broader class of test-time attacks, in which an adversary crafts an adversarial example by perturbing a benign image that causes a misclassification by a ML model. In digital adversarial examples, adversary’s goal is for the perturbed image and the benign image to look the same to a human. For physical adversarial attacks (the topic of this paper), adversary’s goal is two fold: (1) Make a change to a small area of the object, e.g., place some stickers on the object; and (2) for the resulting perturbed image to survive physical transformations (e.g. perturbed stop sign should appear as a speed limit sign from various angles and distances). Even though a growing body of recent work has focused on creating robust physical adversarial examples, where an attacker manufactures a physical object with special

perturbations [13], [14] or modifies existing objects with manufactured elements such as stickers [15], [16], [17], there are two limitations of current approaches. First, the existing body of work assumes access to a white-box model where gradient information is available [14], [15]. Second, finding good candidates for robust physical attacks still requires a fair amount of hand-crafting, e.g., identifying a good area in the image to apply a perturbation and then searching for an optimal perturbation.

We address both limitations in our novel algorithm, GRAPHITE (Gradient-free Robust Adversarial Physical Hard-label Image-based Targeted Examples). GRAPHITE assumes a *hard-label* threat model that more closely mirrors real-world deployments of ML [18] — many commercial or proprietary systems are closed source, and only provide answers to prediction queries. GRAPHITE also proposes a multi-objective optimization formulation of the problem that addresses the twin objectives of perturbing only a small, but unknown, fraction of an image and making the perturbation misclassify to a desired target label with a high degree of robustness to viewpoint and lighting changes. As far as we are aware, GRAPHITE is the first algorithm that meets both these objectives. GRAPHITE also does not require access to the training dataset. To find adversarial images, it only requires access to the image to be attacked and an example target image.

The closest approach to ours is the recent work on digital (non-physical) hard-label attacks [18], [19], [20] that, in general, attempt to find a digital adversarial example that is within a small distance from the victim image by doing gradient-free optimization. We experimentally found that these adversarial examples neither have small perturbation areas nor have resiliency to viewing point changes. We found that a radically different approach to optimization is required to generate robust physical perturbations. One of the key innovations in our work is to jointly find a minimal mask and physically robust perturbation in an optimization formulation. This formulation is then solved using a combination of a greedy reduction algorithm to automatically find a viable and small patch area and gradient-free optimization techniques to optimize the patch for increased robustness to physical world variation such as viewpoint changes.

GRAPHITE is designed to generate candidate adversarial patches for images that can be used to simulate physical perturbation attacks on objects such as traffic signs. Similar to Eykholt et al. [15], we did field testing of several attacks



Fig. 1: Targeted GTSRB attack to convert a stop sign into a speed limit 30 km/hr sign, generated by GRAPHITE.

by creating adversarial perturbation stickers, put them on real objects, and measured the success rate of the attack under different angles and distances in lab and drive-by tests. In general, we found that the adversarial attacks identified by GRAPHITE worked well in the real-world. For example, we printed out and applied a candidate adversarial patch generated by GRAPHITE to a real stop sign and found that the stop sign was detected as a speed limit 30 km/hr sign 92.86% of the time under varying viewpoints and lighting conditions.

Generating adversarial images with GRAPHITE currently takes about several minutes. Nevertheless, an advantage of GRAPHITE over prior work is that it is *fully automatic*, with no intermediate manual steps in generating small adversarial patches that are designed to be resilient to viewpoint changes. Designing such algorithms that are fully automated and do not require hand-crafting is important for being able to incorporate the attack-generation algorithms into adversarial training algorithms to help defend against physical perturbation attacks. Fig. 1 shows an example GTSRB attack.

Our Contributions:

- We introduce, to the best of our knowledge, the first hard-label algorithm for creating candidate physical adversarial examples. As far as we are aware, GRAPHITE is the first algorithm that automatically finds both small masks and achieves high robustness to environmental transforms in either white-box or black-box settings.
- We provide a formulation of a joint optimization problem across masks and robustness of the classification to environmental transforms. We show that the problem is computationally hard. We present algorithms to address it and include theoretical analysis of the algorithms.
- We evaluate GRAPHITE on multiple (victim, target) pairs on the GTSRB dataset and found that it succeeded in finding perturbations with both small mask area and high robustness, based on expectation over transforms (EOT) metrics proposed by Athalye et al. [14]. We also confirm the robustness of attacks in physical settings by applying

stickers to a stop sign, as suggested by GRAPHITE, using the evaluation methodology of Eykholt et al. [15].

II. BACKGROUND

We discuss our threat model and background information on attack algorithms.

A. Threat Model

We focus on hard-label, decision-based attacks in the physical world. We assume the attacker can only access the classification output (i.e., the highest confidence class label) without any confidence information. This type of threat model is most relevant to CPSs, where an attacker can easily obtain query access to the ML models without having to spend extra effort to reverse engineer a full neural network. Furthermore, we assume that the attacker can modify the physical appearance of a target object by placing stickers on it.

B. Adversarial Attacks in White-Box settings

Szegedy et al. [6] showed that small imperceptible perturbations δ on an input x can be found that lead to misclassification of deep neural networks. Such small perturbations can be automatically determined by solving the following optimization problem:

$$\operatorname{argmin}_{\delta \in \mathcal{S}} \nu(\delta)$$

$$F(\theta, x + \delta) = y_{adv}$$

where \mathcal{S} is allowed perturbation space, ν is an appropriate norm, F is the classifier, θ are the model parameters, and y_{adv} is the adversary's desired target label (we assume a targeted attack). If the model parameters are clear from the context, we will simply write the classifier's output on x as $F(x)$. In white-box settings, given a model with parameters θ , a perturbed input can be computed using gradient information. Several targeted attacks exist in the literature [12].

C. Adversarial Attacks in Soft-label Black-Box Settings

If white-box access to the model is not available, then it is not straightforward to compute the gradient $\nabla_x L(\theta, x, y)$, since the adversary does not have access to the model $F(\theta, x)$. One approach is to instead use *score-based* techniques that rely on the access to the softmax layer output in addition to the final class labels [21], [22]. Zeroth-order gradient estimation techniques are then used to estimate the gradient. In particular, the softmax layer output is used to estimate the change in loss on a set of random perturbations around x , which can then be used to estimate the gradient [21], [22].

D. Adversarial Attacks in Hard-label Black-box Settings

A recent line of work has started exploring hard-label attacks in the digital setting [18], [19], [20], [23] in which the adversary has access to neither the soft labels nor the model – the only access is to the top-1 label. Hard-label settings are more challenging for an adversary because hard labels create a discontinuous optimization space – most perturbations will likely simply return the same label and thus it becomes

difficult to figure out the best direction in which to do the perturbation. Thus, zeroth order gradient estimation used in soft-label black-box settings fails.

Cheng et al. introduced the algorithm OPT-attack [18] to address the discontinuous optimization space problem. Let x refer to a victim image that we, as attackers, wish to be classified by the model F as an image in the target class y_{adv} . The perturbation that causes this classification change can be thought of as an adversarial direction ϕ . OPT-attack aims to find the perturbation direction ϕ that has the least distance to the decision boundary. Let λ refer to a scaling factor and let $g(\phi)$ be the scalar distance to nearest adversarial example in the direction ϕ . Formally, this leads to the following optimization problem:

$$\min_{\phi} g(\phi) \quad (1)$$

where the objective $g(\phi)$ is defined as:

$$\min_{\lambda > 0} \lambda \text{ s.t. } \left(F \left(x + \lambda \frac{\phi}{\|\phi\|_2} \right) = y_{adv} \right) \quad (2)$$

In [18], the attacker initializes ϕ to be the minimal pixel-wise difference between the starting image x and a random target class image from the training set. Note that OPT-attack requires a valid target example for proper initialization and then works towards reducing the distance from the original image. Generally, OPT-attack is set up to generate and update noise in the dimension of the model input, which matches the training set and initial attack images.

Once ϕ has been initialized from an example target class image, OPT-attack finds $g(\phi)$ by doing a binary search in the direction ϕ to find the nearest point around which the decision flips from the victim to the target. Once one $g(\phi)$ is found, the algorithm proceeds to find other decision boundary points in nearby directions to optimize $g(\phi)$ with zeroth-order optimization. Specifically, Cheng et al. [18] use the Randomized Gradient Free (RGF) method [24], [25], though other zero-order methods can also be used to estimate the gradient. At a high-level, the algorithm samples nearby directions and uses that to estimate a gradient to use in the optimization. The gradient update is defined as an average of q gradient calculations \hat{g} , where

$$\hat{g} = \frac{g(\phi + \beta u) - g(\phi)}{\beta} \cdot u \quad (3)$$

In the above equation, u is a normalized, random Gaussian vector and β is a nonzero smoothing parameter.

E. Robust Physical Perturbation Attacks

Prior work has shown that standard digital adversarial examples fail to be robust under environmental variations [26], [27]. Athalye et al. introduced the idea of environmental transforms to account for varying conditions such as the distance and angle of the camera, lighting conditions, etc. and recommended changing the objective function to maximize the robustness across the space of environmental transforms

[14]. Consider a distribution of environmental transforms T that transform x to alternative viewpoints or to different lighting conditions under which we aim to achieve robustness. Then, the revised optimization objective, given a model to be attacked with parameters θ , is as follows:

$$\operatorname{argmin}_{\delta \in S} \nu(\delta) + \mathbb{E}_{t \sim T} \left[F(\theta, t(x + \delta)) \neq y_{adv} \right] \quad (4)$$

The expected value of loss under the full space of possible transformations is challenging to determine. Athalye et al. referred to this average loss value as *EOT* (expectation over transforms) and estimated it by averaging loss over 40 random digital transforms. Athalye et al. printed the adversarial images and re-captured them with camera and confirmed that adversarial images with high EOT values tended to have high robustness (i.e., were misclassified) while those with low EOT values and those generated without factoring in transforms tended to have low robustness. *Thus, EOT can serve as a reasonable proxy to physical-world validation, which tends to be expensive.*

From now on in the paper, we will use a more descriptive term, *survivability*, to refer to EOT since the goal of high EOT is to ensure survival of classification under different environmental conditions.

Athalye et al. [14] addressed the issue of physical robustness of adversarial examples but they were not designed to perturb existing objects in the real world. Eykholt et al. [15] extended the EOT work to find perturbations that could be physically realized and placed on real-world objects such as traffic signs to cause a change in classification. A key element to find such examples was the notion of a *mask* that constrained the perturbation to a limited area of the sign and was defined by a matrix of 0's and 1's of the same size as the input image. In [15], such masks were crafted manually and then, once a mask M_x was chosen for an input x , the following optimization problem was solved:

$$\operatorname{argmin}_{\delta \in S} \nu(\delta) + \mathbb{E}_{t \sim T} \left[F(\theta, t(x + M_x \cdot \delta)) \neq y_{adv} \right] \quad (5)$$

In contrast to digital attacks and even the work of Athalye et al. [14], the perturbation δ itself was unconstrained, except for it being required to be confined to the mask area M_x . Eykholt et al. [15] did not provide a procedure for automatically identifying a good mask M_x or for evaluating them, but they provided some suggestions, e.g., they recommended finding perturbations based on the l_1 norm to help identify areas in an input image that were likely to be most sensitive to changes. Thus, even though robust physical perturbation attacks on machine learning models have been convincingly demonstrated on some examples, *actually finding good candidates for such attacks efficiently remains an art*, even in white-box settings. As far as we are aware, there is no automated procedure currently available.



(a) Victim sign (b) Target sign (c) Vanilla OPT (d) Robust OPT

Fig. 2: Results from OPT on a targeted attack from stop sign (a) to a German 30 speed limit sign (b). Adversarial image (c) from vanilla OPT has poor survivability under digital environmental transforms. Adversarial image (d) is generated by OPT after incorporating a 80% expected survivability under transforms goal, but has obvious artifacts from the target image. Both adversarial images would be hard to use in the physical world without covering or replacing an entire sign.

F. Initial Strawman Approach

We tried vanilla OPT to do a targeted attack to convert a stop sign (Fig. 2a) to a German speed limit 30 km/hr sign (Fig. 2b) in the GTSRB dataset. The result is shown in Fig. 2c. The attack results in modification of over 90% of the pixels and has less than 1% digital survivability under environmental transforms (transforms used to measure survivability are discussed later in Experiments).

We then incorporated Athalye’s EOT (survivability) measure into the optimization by defining a wrapper function $F'(x)$ as follows, aiming for 80% survivability:

$$F'(x) = \begin{cases} y & \text{if } \mathbb{E}_{t \sim T} \left[F(t(x + \delta)) = y \right] \geq 80\% \\ -1 & \text{otherwise} \end{cases} \quad (6)$$

In the above, -1 is a special value indicating that the result has insufficient survivability. The resulting image from OPT on optimizing the attack for $F'(x)$ is shown in Fig. 2d. The results in Fig. 2c and 2d can vary depending on the initial random seed used in OPT but, in general, we found OPT applied to $F'(x)$ yielded poor results with significant artifacts from the target sign visible. The problem we are addressing in this paper is even harder since we also need to confine that attack to a small yet-to-be-determined area of the stop sign.

We also considered manually crafting masks (as in Eykholt et al. [15]) and trying OPT in the masked region, but there are two problems. The first one is finding a suitable mask that results in $F'(x)$ being the target label with the desired survivability (e.g., 80%). Assuming that can be done (a hard problem), OPT is still likely to exhibit target artifacts in the mask region. As an example, using the mask from RP_2 yielded an initial survivability of less than 1% when using our stop sign and speed limit 30 km/hr images as the victim and target and OPT failed to initialize.

III. OPTIMIZATION FOR HARD-LABEL PHYSICAL ATTACKS

In this section, we will describe our approach, GRAPHITE. Unlike prior work, our goal is to both find a candidate mask

and the perturbation within that masked area so that the resulting image is likely to be robust when physically realized. We will first describe a joint optimization problem for finding an optimal perturbation and mask and then discuss our approach to solving it in hard-label blackbox settings. As in Athalye et al. [14], we also rely on estimating *survivability* of an image under transforms, i.e., expectation of an image being predicted with a given label under physical world transformations (this was termed EOT in Athalye et al. [14]).

A. Problem Setup

In our approach, our goal is to find some perturbation δ and a small mask M such that when δ is applied to a victim image x our model F predicts the target label with high survivability. The area that δ may occupy is constrained by the mask M . The perturbations must have high expected survivability under transformations t sampled from a distribution T . To help with initialization, we will utilize an example target image x_{tar} . We also introduce a general mask goodness function $h(M)$ that rewards masks that have configurable desirable properties, such as masks with a guaranteed minimum survivability or masks that have a certain shape.

B. Joint Optimization

With the notation above, we will first describe our new joint optimization problem. The optimal noise must maximize survivability and take up as little of the sign as possible. These goals are in opposition and must be solved jointly to achieve the best solution.

$$\begin{aligned} \underset{\delta, M}{\operatorname{argmin}} \quad & \lambda_1 \cdot \|M\|_0 + \lambda_2 \cdot h(M) \\ & + \mathbb{E}_{t \sim T} \left[F(t(x + M \cdot \delta)) \neq y_{adv} \right] \\ \text{s.t.} \quad & \forall_i M[i] \in \{0, 1\} \end{aligned} \quad (7)$$

We argue that solving this directly is computationally challenging, especially in the hard-label setting. The first reason is that finding an optimally-sized mask by itself is a combinatorially hard problem (we include a proof in the Appendix to show that it is NP-complete).

Secondly, we also operate in a very large discrete and discontinuous space when examining hard-label attacks. Somehow, we must find a reasonable way to map the problem to a form so that we apply gradient free methods or otherwise optimize this space.

Given that we have established that solving the above problem of joint optimization is both combinatorially hard (due to the notion of a mask) and difficult to characterize purely in terms of gradients, we solve a decoupled optimization problem and apply some heuristics to find good solutions.

IV. GRAPHITE’S TWO-STAGE APPROACH

We now describe our two-stage formulation where we first find a good candidate mask heuristically (given that solving the optimal problem is NP-hard; see Appendix) and then find an optimal perturbation to put within that mask.

A. Mask Generation Optimization Problem

We first find an optimized mask which when filled in with the target image x_{tar} results in a minimum specified level of survivability. We constrain the perturbation to be fixed at $\delta_{tar} = x_{tar} - x$ and solve the optimization objective from (7) under that constraint:

$$\begin{aligned} \underset{M}{\operatorname{argmin}} \quad & \lambda_1 \cdot \|M\|_0 + \lambda_2 \cdot h(M) \\ & + \mathbb{E}_{t \sim T} \left[F\left(t(x + M \cdot \delta_{tar})\right) \neq y_{adv} \right] \\ \text{s.t.} \quad & \forall_i M[i] \in \{0, 1\} \end{aligned} \quad (8)$$

We show how to solve this formulation heuristically using an algorithm described in Section V-A.

B. Perturbation Generation Optimization Problem

Equipped with the mask M found by the Mask Generation Optimization Problem, we then aim to maximize survivability for the given mask. This is given by the last quantity in our joint optimization problem (7) and is given by the objective function below:

$$\underset{\delta}{\operatorname{argmin}} \quad \mathbb{E}_{t \sim T} \left[F\left(t(x + M \cdot \delta) \neq y_{adv}\right) \right] \quad (9)$$

We note that the above is equivalent to finding a perturbation that maximizes the survivability with respect to the target label:

$$\underset{\delta}{\operatorname{argmax}} \quad \mathbb{E}_{t \sim T} \left[F\left(t(x + M \cdot \delta) = y_{adv}\right) \right] \quad (10)$$

By using survivability as a measure of physical robustness, we can leverage this function as an optimization goal we can pursue even in the hard-label case (described in Section V-B). Later, in Section V-C3 we provide empirical evidence to suggest that this function has relatively low Lipschitz constants even when approximating the expectation in (10) by averaging over n transformations. We additionally refer to this process as *boosting* the survivability, as we start with a δ with lower survivability and attempt to boost it as high as we can.

V. GENERATING HARD-LABEL PHYSICAL ATTACKS WITH GRAPHITE

We now describe how to solve the mask and perturbation generation problems presented in Section IV in the hard-label setting. For ease of algorithmic notation, given a mask M and perturbation δ the survivability in (10) can be estimated as follows by computing n randomly sampled transforms $t_i \sim T$:

$$S(M, \delta) = \frac{\sum_{i=1}^n \mathbb{1} \left[F\left(t_i(x + M \cdot \delta)\right) = y_{adv} \right]}{n} \quad (11)$$

Fig. 3 shows the algorithm flow along with intermediate and final results. The figure covers the mask generation and boosting phases we will discuss next.

A. Mask Generation

We need to find a candidate mask that has good initial survivability and small size. Boosting (described in V-B) can take care of further improving the survivability.

We generate masks using a three stage process:

- 1) Heatmap Estimation
- 2) Coarse-grained Mask Reduction
- 3) Fine-grained Mask Reduction

We initialize the mask to cover the entire victim object with the target object. We then choose a group of pixels called a *patch* as a configurable input into the algorithm. In our experiments, for 32×32 images, we chose a 4×4 square patch. The patch serves two purposes: (1) it helps us estimate a heatmap (i.e., which pixels contribute more to survivability) and (2) it is used to punch holes in the mask to reduce the number of pixels as the algorithm progresses while optimizing the mask objective function (8). Choosing a very small patch (e.g., 1 pixel) was not ideal from two perspectives: heatmap estimation was less effective because removing a single pixel has minimal impact on survivability and punching 1-pixel holes makes it harder to eventually print out the final image and cut holes in it for physical realization. A 4×4 square patch in pixels corresponded to roughly $4'' \times 4''$ square on a physical 30'' stop sign. In principle, any other patch shape could have been used, potentially giving additional attack images.

1) *Heatmap Estimation*: We begin by estimating the impact of removing one patch at a time at each possible position in the initial mask and then measuring the resulting target's survivability. If the survivability remains high after patch removal, those pixels are likely unimportant to inducing a target prediction. In contrast, the more the survivability drops, the more important the patch area is to inducing a target prediction.

In general, the heatmap is a function of the point at which it is estimated. For instance, Fig. 4a shows the heatmap with respect to the target and Fig. 4b shows the heatmap relative to the victim (we measure the heatmap by adding a patch in the latter case and measuring the drop in survivability with respect to the stop sign – survivability of the target label tended to remain 0 and not sufficiently interesting. In principle, the heatmap could be measured at multiple points during the algorithm, but the measurement is expensive in terms of number of queries and computation time. Empirically, we found that just using one heatmap (in our case, the target one) worked well in practice. The white area in Fig. 4a is interesting – it suggests that area is likely to be crucial for applying a patch in order to convert the stop sign to the speed limit 30 km/hr sign. Conversely, darker areas in Fig. 4a are good candidates for elimination from the mask.

2) *Coarse-grained Mask Reduction*: Utilizing the information in the heatmap (assumed to be relative to the target as shown in Fig. 4a), we want to begin reducing the size of the mask. The reduce algorithm first sorts all the patches for each position in the heatmap in decreasing order of survivability (i.e., from least impactful to most impactful).

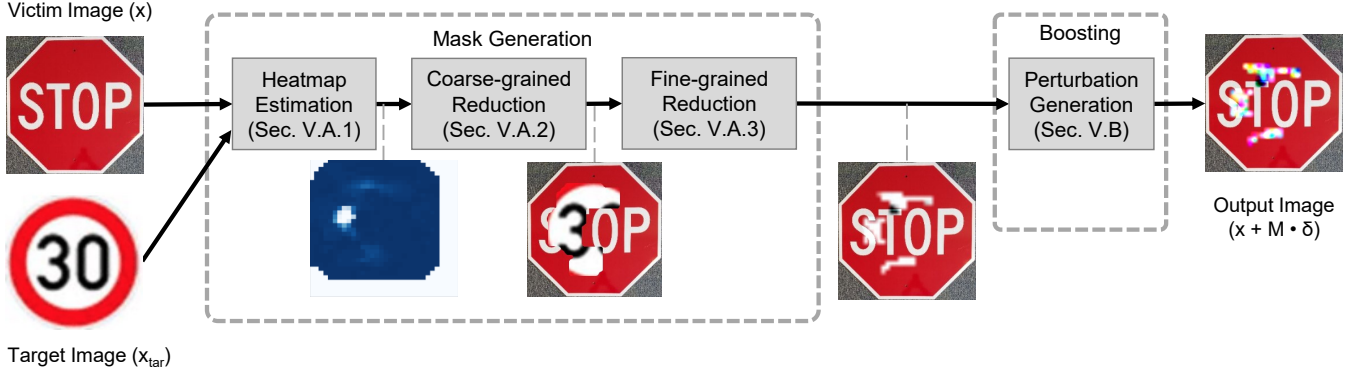


Fig. 3: Figure showing the algorithm flow with intermediate and final results for a targeted attack on a stop sign to 30 speed limit sign.

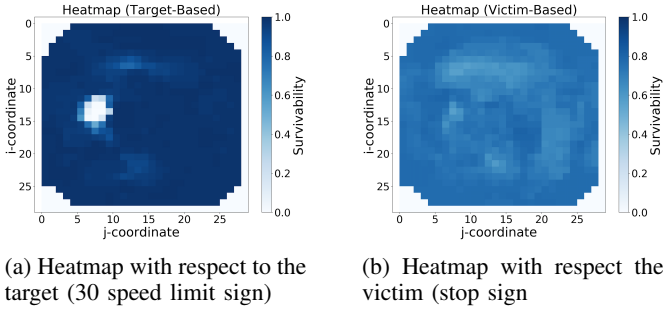


Fig. 4: Example heatmaps.

Thus, the lighter regions in Fig. 4a will appear later in the sorted list. As an optimization to save queries, we do a coarse-grained pruning initially. We posit that the order of patches from least impactful to most impactful is highly reflective of the probability of inclusion of these patches in the final mask. Thus, we initially do a fast reduction of our mask through binary search. Specifically, we find the point in the ordered queue of patches \mathcal{P} such that the bitwise union of all of patches with greater impact yields a mask of survivability $\geq s_{hi}$, where s_{hi} is a high threshold that must be hit in the initialization and is a hyper-parameter. If s_{hi} cannot be reached, we simply include all patches. Compared to starting with the full object covering mask and reducing patches one by one, this initialization process allows us to cut out the low impact patches faster and in a coarse-grained manner.

3) *Fine-grained Mask Reduction*: We then execute a fine-grained *reduction* that uses a greedy algorithm to improve the objective score of (8). The algorithm starts from low impact patches (i.e., low impact on target survivability) to more impactful patches and greedily removes patches if it improves the objective function. Conceptually, this objective function can be anything that rewards smaller masks and penalizes low survivability. We propose the base objective (or scoring function) from (8) where $h(M)$ is simply a Boolean constraint that imposes a high penalty for survivability below the low

threshold s_{lo} (a hyper-parameter) and does nothing otherwise. We will discuss other objective functions in Section VII, but suggest that functions rewarding or penalizing certain characteristics or the mask (e.g. a minimum survivability, minimum size, or shape constraint) could be used instead. We let the overall objective function in (8) be referred to as a mask score function J .

An interesting question is whether the fine-grained approach is even required. We later show in experimental results that coarse-grained reduction by itself does not produce good results (it leads to significantly larger masks). Score-based pruning generally requires queries to measure survivability since that is one of the factors in the score. One likely reason fine-grained reduction helps is that the initial heatmap is not necessarily perfectly accurate as the mask is pruned.

A future direction is to explore other heuristics other than greedy. We considered hill-climbing algorithm as a potential alternative in which we make multiple passes over the list of remaining patches and try to apply them until no further patches can be applied to improve the score. This guarantees a local minimum (since the problem is likely non-convex), but significantly increases the query cost since testing each patch application for survivability, which is needed to evaluate the score, involves n queries (see Equation 11). Empirically, we found greedy approach to provide satisfactory solutions.

Let n be the number of transforms and \mathcal{P} be the set of valid patches. The number of queries is then bounded by $O(n \cdot |\mathcal{P}|)$. In the worst case, we make two full passes over each patch (once for heatmap estimation and once in reduction), plus at most $\log |\mathcal{P}|$ queries for a binary search. The algorithm in full is presented in Algorithm 1.

An example output and algorithm flow for the mask generation phase is in Fig. 3. The resulting image after this phase consists of the victim image outside the generated mask M and the target image inside the mask, i.e., the resulting image at this stage is $x + M \cdot (x_{tar} - x)$.

Algorithm 1: Algorithm to generate mask. Compute heatmap estimate of each patch in the object, sort patches, greedily remove patches that improve the score function J , which tries to minimize number of pixels in mask, minimize sparsity, and minimize error. Value for λ_1 is found through hypertuning.

Input : x, x_{tar}, y_{adv}

Output: M with lowest mask score $J(M, \delta, s_{lo})$

```

1 Function  $\mathcal{J}(M, \delta, s_{lo})$  :
2   if  $S(M, \delta) < s_{lo}$  then
3     return  $\infty$ 
4   return  $\lambda_1 \cdot \|M\|_0 + (1 - S(M, x_{tar} - x))$ 
5
6 Function GenMask( $x, x_{tar}, s_{lo}, s_{hi}$ ) :
7    $\mathcal{P} \leftarrow$  Set of all patches
8    $M \leftarrow$  Mask covering the whole object
9   // HEATMAP ESTIMATION
10  for  $\rho$  in  $\mathcal{P}$  do
11     $s_\rho \leftarrow S(M - \rho, x_{tar} - x)$ 
12  end
13  Sort  $\mathcal{P}$  from highest  $s_\rho$  to lowest
14  // COARSE REDUCTION
15   $i \leftarrow$  Binary search for highest index such that
     $S(M^*, x_{tar} - x) \geq s_{hi}$ , where  $M^*$  is the bitwise
    union of all patches  $\rho_i$  to  $\rho_{|\mathcal{P}|}$ 
16   $M \leftarrow M^*$ 
17  // FINE REDUCTION
18  for  $\rho$  in  $\mathcal{P}$  do
19    if  $J(M - \rho, x_{tar} - x, s_{lo}) < J(M, x_{tar} - x, s_{lo})$ 
    then
20       $M \leftarrow M - \rho$ 
21    end
22  end
23  return  $M$ 

```

B. Perturbation Generation (Survivability Boosting)

Given a resulting image x and a mask M from the previous stage, survivability boosting, or simply boosting, aims to find the perturbation δ to add to x to create a targeted adversarial example for class y_{adv} that can survive physical-world transformations with the highest probability (see Equation 10). By directly optimizing over *survivability* with respect to the target label, we aim to create robust physical attacks that are constrained to a perturbation space defined by the mask M . Survivability also gives us a function whose gradient we can estimate. We use the Randomized Gradient Free (RGF) method [24], [25] to find maximally robust perturbations.

Our perturbation generation process has several crucial differences from OPT-style attacks [18]. The first is that we have a survivability based re-formulation instead of a distance based re-formulation. We use the initial target example x_{tar} to initialize the noise and then begin maximizing survivability, whereas OPT-attack interpolates between victim and target to find the boundary, and then effectively searches near the

Algorithm 2: Algorithm to generate perturbations for a given mask. Goal is to attack victim image x to be classified as target y_{adv} with the use of example target image x_{tar} , mask M . Hyper-parameter values given in Section VI-A.

Input : $x, x_{tar}, M, b, q, \beta, \eta$

Output: δ with highest survivability

```

1  $\delta \leftarrow x_t - x_v$ 
2  $s \leftarrow S(M, \delta)$ 
3 while  $\text{num queries} + \text{iteration cost} \leq b$  do
4   # Estimate Gradient
5   for  $i = 1 \dots q$  do
6      $u_i \leftarrow$  random, normally distributed vector of
        dimension  $|M|$ 
7      $s_i \leftarrow S(M, \delta + \beta \cdot u_i)$ 
8      $\hat{g}_i = \frac{s_i - s}{\beta} \cdot u_i$ 
9   end
10   $\hat{g} =$  Average of  $\hat{g}_i$  values
11  # Update
12   $\delta \leftarrow \delta - \eta \cdot \hat{g}$ 
13   $s \leftarrow S(M, \delta)$ 
14 end
15 return  $\delta$  with highest  $s$ 

```

boundary to find closer points to the victim. We do not need to find such a boundary or search around the boundary.

Another key difference is that OPT-attack requires frequent calculations of the boundary distance, which is calculated through binary search and is query-intensive. Our survivability metric is computed directly on the n transformation samples and does not require binary searching to estimate a boundary distance.

Once δ has been initialized $M \cdot (x_{tar} - x)$, we proceed to maximize the probability that a perturbation will remain robust to physical-world transforms with the RGF [24], [25] method for gradient estimation using q random samples for each gradient estimation. Explicitly, let u be random Gaussian unit vectors within the allowable range of the mask. Then, the gradient update is as follows:

$$\hat{g} = \frac{S(M, \delta + \beta u) - S(M, \delta)}{\beta} \cdot u \quad (12)$$

To ensure query efficiency, we also impose a query budget b on the boosting stage. The complete algorithm is presented in Algorithm 2.

C. Theoretical Analysis

GRAPHITE has two main sources of error that can affect the perturbation quality: (a) Sampling error: we sample a set of transformations to estimate a solution to Equation (10) and (b) GFO error: in the hard label setting, the attacker does not have access to gradient information. GRAPHITE uses gradient-free optimization that samples a range of random Gaussian vectors leading to errors in gradient estimation. In

this section, we provide an analysis of these two errors. We first show that solving the approximation approaches the true solution given enough sampled transformations implying that sampling introduces a very low error in the optimum with high probability. Second, for a fixed error in perturbation value, the number of boosting iterations (Sec. V-B) that GRAPHITE needs is proportional to the Lipschitz constant of the objective function. Section V-C3 contains experimental results showing that our objective has a low Lipschitz constant without big jumps.

1) *Sampling Error Bounds*: Let δ_1 be the solution to (10) and δ_2 be the solution to version estimated over n samples. Then we have the following:

With probability at least $1 - 2e^{-\frac{nq^3}{3\epsilon^2}}$ we have that $|G(\delta_1) - G'(\delta_2)| < \epsilon$, where G and G' is the function being optimized in (10) and a version of (10) approximated with n transforms respectively.

With the requisite choice of n and ϵ we can make the probability $1 - 2e^{-\frac{nq^3}{3\epsilon^2}}$ very close to one. Intuitively, it means that *with high probability sampling introduces a very small error in the value of the optimum*. We provide a complete proof for the statement mentioned above in Appendix B.

2) *GFO Error*: We give some background on *gradient-free optimization (GFO)*. For details we refer to [24]. Let $f : E \rightarrow \mathbb{R}$ be a function, where $E = \mathbb{R}^n$. Define its Gaussian approximation $f_\mu(x)$ as follows:

$$f_\mu(x) = \int_E f(x + \mu u) p_N(u) du \quad (13)$$

Where $p_N(u)$ is the probability-density function (pdf) a n -dimensional multi-variate Gaussian $\mathcal{N}(0, \Sigma)$. In GFO, one replaces the gradient of f in the descent procedure to find the optimum of $g_\mu(x)$ as follows: pick u distributed according $\mathcal{N}(0, \Sigma)$ and define it as:

$$\frac{f(x + \mu u) - f(x)}{\mu} \cdot \Sigma^{-1} \cdot u \quad (14)$$

In other words we take a directional derivative in the direction of a random Gaussian. Note that the derivative can be evaluated by black-box queries on f . Further note that the function we are optimizing is not convex and also might not be differentiable, so we are in the second case of [24, Section 7]. Essentially the number of iterations needed to achieve a certain error is proportional to the Lipschitz constant of the function f .

3) *Lipschitz constants*: To demonstrate that our object has a low local Lipschitz constant, we execute boosting on an example stop sign to speed limit 30 km/hr attack with $n = 1000$ transformations and approximate the local Lipschitz constant every time we compute $S(M, \delta + \beta \cdot u)$. The approximate local Lipschitz constant is given by $\frac{|S(M, \delta + \beta \cdot u) - S(\delta)|}{|\beta \cdot u|}$. We found that the maximum observed local Lipschitz constant was 0.0537. Figure 5 shows a histogram of observed local Lipschitz constant, and we can see the majority of these values are very low. From the previous section it is clear that low local Lipschitz constants lead to better convergence.

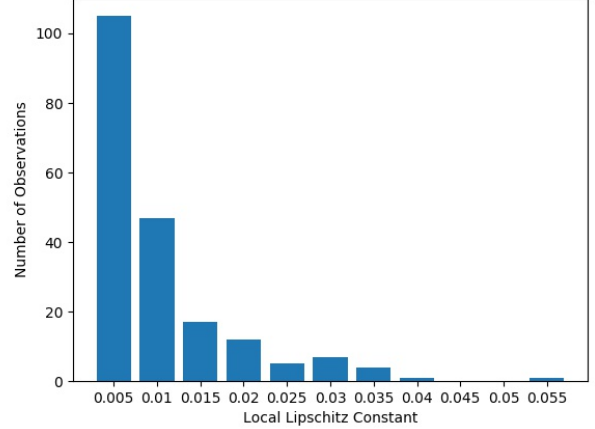


Fig. 5: This figures shows a histogram of our approximate local Lipschitz constant observations on survivability. The constants are binned in intervals of 0.005 with the label being the right side of the interval. This graph shows that survivability does not vary too much per amount of change.

VI. EXPERIMENTS

We demonstrate the viability of GRAPHITE by attacking a traffic sign classifier trained on German Traffic Sign Recognition Benchmark (GTSRB) [28] data. We show that our results are robust to physical world transforms. We do this by both reporting *digital survivability* results on a broader range of attacks and a subset of *physical survivability* results to confirm that our digitally robust examples translate to the physical world in the form of stickers. We also show results in a drive-by setting, similar to Eykholt et al. [15].

A. Experimental Setup

Datasets and Classifiers. We use the classifier from RP₂ [15], [29] trained on an augmented GTSRB dataset [28]. Similar to RP₂ [15], we replace the German stop signs with U.S. stop signs from the LISA dataset [30]. As a validation set, we take out the last 10% from each class in the training set. We also augment the dataset with random rotation, translation, and shear, following Eykholt et al. [15]. Our network, GTSRB-Net, has a 97.656% accuracy on the test set.

In both attacks, we use our own victim image of the source object and use an Internet image outside of the dataset for initialization to demonstrate that GRAPHITE does not rely on having training set images to initialize from. In our experiments we assume that object boundaries are available, but note they could be obtained automatically through an object segmentation network [31].

Hyper-parameters. We set $\beta = 1$, $\eta = 500$, and the query budget b to 20k. In both approaches, we test over $n = 100$ transformations and take $q = 10$ gradient samples. Once we have a final attack, we re-evaluate the survivability over $n = 1000$ transforms to get a better estimate of how well it will

perform. In practice, the difference between survivability on 100 vs. 1000 transformations was often within 3%.

For transformations, we model rotation about the y axis with homography matrices, lighting changes with gamma correction, and focus changes with Gaussian blurring. For our GTSRB [28] attack we set rotation about the y axis to be between -50° and 50° and fix the base focal length $f = 3$ ft. The projected image plane distance is allowed to vary between f and 15 ft. Crop sizes and offsets can vary between 0% and 3.125%. The max γ effect can be 3.5 for darkening (or $\frac{1}{3.5}$ for lightening), and use Gaussian kernels of size 1, 5, and 9. All parameters are sampled uniformly. We discuss in more detail our process of doing transformations in Appendix C.

B. Digital Survivability Tests

We report a subset of results when run with a high threshold $s_{hi} = 90\%$ for coarse-grained mask reduction and a low threshold $s_{lo} = 70\%$ for fine-grained mask reduction. We note that a higher s_{hi} helps ensure that the coarse-grained reducer does not remove useful patches while a higher s_{lo} increases the odds that the final boosted survivability is higher, as it provides a better starting point. We note that these parameters can be tuned based on the specific victim target pairs and to tradeoff more subtle noise and survivability, which we discuss further in Section VII.

In this section, we generate attacks with $n = 100$ transformations during the attack and then calculate the final survivability on $n = 1000$ transformations. A sample of results are shown in Table I. We show that we can attack with a variety of victim and target pairs and achieve greater than 75% survivability, with often 10% or less of the original object perturbed.

Fig. 6 shows the trends of survivability and number of pixels over time as the algorithm runs where the victim image is a stop sign and the target is a speed limit 30 km/hr sign. Generally speaking, the survivability drops some as we generate a mask and then once we have a mask we boost the survivability up with gradient-free optimization. We noticed an unexpected drop in survivability around 475 seconds as the algorithm was transitioning from the reduce phase to boost phase. It turned out that this was due to statistical estimation of survivability over 100 random transforms. The boost phase made its own estimate of initial survivability, which turned out to be slightly lower than the survivability estimated by the reduce phase. This variance is one reason why we estimate the final survivability in our experiments using 1000 transforms.

We additionally present an ablative study over different reduction strategies in mask generation to enforce a specific minimum survivability threshold. The results are shown in Table II. For these results we attack a stop sign to become a speed limit 30 km/hr sign under three settings: the full mask generation pipeline, only reducing the mask in a coarse-grained manner, and only reducing the mask in a fine-grained manner. The minimum threshold is 70%.

These results show that both reduction processes have benefit. While using only fine-grained reduction yields similar

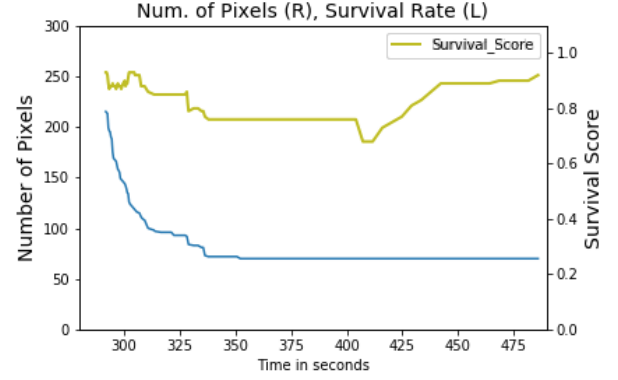


Fig. 6: The above plot shows the three phases of the algorithm. The plot starts near time 286 because it takes approximately 286 seconds to build up a heatmap. The binary search stage is very quick and reduces the number of pixels in the mask from 702 to 215 with a survivability of 90%. Over the next 113 seconds, the reduce stage further reduces the number of bits in the mask to 70 bits and estimated survivability to 76%. The boost stage starts at approximately 475 seconds. It boosts the survivability to 93% while keeping the same number of bits. further reduces the number of bits to 70 with a survivability of 70%.

survivability and mask size results to the full algorithm, it uses almost 10k more queries and takes some more time. When only using coarse grained reduction, many more pixels are included to reach the same minimum 70% threshold, and thus these masks are much larger.

C. Physical Robustness Lab Tests

The findings by Athalye et al. [14] and Eykholt et al. [15] suggest that digital survivability can be a good proxy for physical survivability. We carried out physical object perturbation experiments in the field and generally confirmed those findings. We evaluate GRAPHITE on a targeted attack with a victim image of a stop sign with a target label of speed limit 30 km/hr at different viewing angles and lighting conditions.

We set the size of our original image to be 244×244 and used 100 randomly chosen transformations in the attack. During the attack, we first generate noise in 32×32 and then upsample to the resolution of the input image whenever they have to be added together.

1) *GTSRB Setup*: We classify our objects at stationary positions to test how robust our attacks are to different viewing conditions. To examine robustness against geometric changes, we take five pictures of the perturbed stop sign at 14 different locations for a total of 70 pictures. To compare against baseline stop sign accuracy, we also take five pictures of a clean stop sign at each of the same 14 locations. The 14 locations were chosen based on RP_2 evaluation [15]. To test lighting conditions, we take one set of images in sunny mid-day conditions and one in the evening with less direct sunlight.

TABLE I: Sample of digital targeted attacks on GTSRB-Net. Ran with $s_{lo} = 70\%$, $s_{hi} = 90\%$, $n = 100$ during attack. Final survivability calculated on $n = 1000$ transformations.















		Target				
						
Victim						
						
Final Survivability			79%	78.7%	84.3%	90%
Mask Pixels			35	75	55	70
Mask to Object Size Ratio			4.99%	10.68%	7.83%	9.97%
						
Survivability			98.1%	95.4%	97.1%	100%
Mask Bits			15	143	63	0
Mask to Object Size Ratio			2.26%	21.54%	9.49%	0%

TABLE II: Ablative study of reduction types. We present final survivability and pixel counts. Attack is stop sign to speed limit 30 km/hr. Full algorithm uses $s_{lo} = 70\%$ and $s_{hi} = 90\%$, only fine reduction uses $s_{lo} = 70\%$, and only coarse reduction uses $s_{hi} = 70\%$

	Final survivability $n = 1000$	Final number of pixels	Queries	Run time
Only Fine Reduction	89.3%	68	131.9k	541.6s
Only Coarse Reduction	89.6%	159	96.0k	397.3s
Full Algorithm	90%	70	123.7k	518.7s

To gather crops we use a YOLOv3 [32] object detector network trained on MS COCO [33] to predict bounding boxes for the stop sign. We take the output bounding boxes, crop the sign accordingly, resize to 32×32 , and send to our network for classification.

We generated an example attack that took approximately 9 mins with a boost budget of 20k queries. In total with mask generation, it used 123.7k queries. It modeled 100 transformations and digitally survived 93% of those transformations by the end. When confirming survivability on 1000 transformations, the attack survived 90% of transformations.

2) *GTSRB Results*: Table III shows the results of the lab tests for our test perturbation, and Table IV shows a subset of images used in the test. We include the percentage of images labeled as speed limit 30 km/hr, the average speed limit 30 km/hr confidence on successes and failures, the average stop confidence over all of the images, and the baseline stop sign results.

Overall, 92.86% of the 140 total images (one set of five at each location mid-day and another set in the evening) were classified as speed limit 30 km/hr. There was not too much variation across either lighting changes or geometric changes, with all spots yielding a successful attack image at least 80% of the time and with little difference between mid-day and evening photos (94.29% vs 91.43%). These results suggest that our perturbations are robust to environmental changes captured by viewing perspectives and lighting. The average confidence is above 85% as well and we confirmed that the speed limit 30 km/hr classifications are due to our stickers, as 100% of baseline images of clean stop signs were correctly classified as a stop sign.

D. Drive-by

1) *Drive-by Test setup*: Boosting can be used alone on a pre-selected mask. We did a drive-by test using a pre-selected mask and then boosting it as in this paper. To evaluate our attack in a driving scenario, similar to Eykholt et al. [15] we record videos of us driving up to the stop sign with a mounted smartphone camera in an empty parking lot. We found 98% of every 10th frames analyzed to be classified as 30 km/hr. In

TABLE III: Lab results of targeted attack (stop sign to speed limit 30 km / hr) on GTSRB-Net under different angles and distances compared against a baseline of clean stop signs. 5 pictures taken at each angle / distance pair listed at mid-day and 5 pictures taken at each angle / distance pair at evening.

Distance / Angle	SL 30 Success (%)	Avg. SL 30 Conf. on Successes	Avg. SL 30 Conf. on Failures	Avg. Stop Conf.	Baseline Stop Success (%)
5' 0°	100%	0.993335	—	0.000247	100%
5' 15°	100%	0.976236	—	0.001119	100%
5' 30°	100%	0.946215	—	0.001646	100%
5' 45°	100%	0.45445	—	0.065648	100%
10' 0°	100%	0.997888	—	0.000366223	100%
10' 15°	100%	0.898794	—	0.0414612	100%
10' 30°	90%	0.885375	0.171763	0.123489	100%
15' 0°	90%	0.861517	0.125965	0.0656558	100%
15' 15°	80%	0.800151	0.0727495	0.157176	100%
20' 0°	80%	0.8663294	0.131629	0.0487754	100%
20' 15°	100%	0.892987	—	0.0052069	100%
25' 0°	90%	0.854974	0.07634	0.00744433	100%
30' 0°	90%	0.946917	0.129826	0.00397451	100%
40' 0°	80%	0.777677	0.0996577	0.0720889	100%
Aggregate (day)	94.29%	0.853619	0.219418	0.0535812	100%
Aggregate (evening)	91.43%	0.886951	0.191157	0.0313188	100%
Aggregate (total)	92.86%	0.870285	0.205288	0.04245	100%

TABLE IV: Sample of lab-test images of targeted attack (stop sign to speed limit 30 km / hr) on GTSRB-Net.








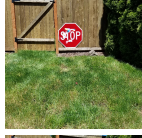
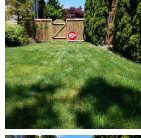


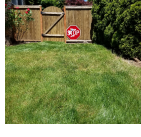


Distance / Angle	Image	Distance / Angle	Image	Distance / Angle	Image
5' 0°		10' 15°		20' 15°	
5' 15°		10' 30°		25' 0°	
5' 30°		15' 0°		30' 0°	
5' 45°		15' 15°		40' 0°	
10' 0°		20' 0°			



Fig. 7: Stop sign to speed limit 30 km/hr drive-by images

contrast, without perturbation applied, the classifier correctly classified the stop sign in all the frames. The adversarial patch applied to a physical stop sign in our tests is shown in Figure 7. This drive-by test was done pre-Covid-19 and before the mask generation algorithm was in place. Later experiments with GRAPHITE’s patches automatic mask generation were done in one of the author’s backyard (Tables III and IV).

VII. DISCUSSION AND LIMITATIONS

Our mask generation process introduces the notion of a scoring function, which gives the user valuable flexibility to optimize their physical perturbations to fulfill different objectives. For example, different weights could favor either smaller masks or higher survivability. The score function can also be used to impose constraints such as finding masks that are smaller than some percent of the object area, or requiring that the starting survivability be at least some percent. The objective could also be adaptively applied. We posit that our default score function is useful for most cases and provide it as a way to automate attacks, but our approach lends some flexibility for fine-tuning on specific cases.

We found that good thresholds s_{lo} and s_{hi} can be different across varied attack pairs. This means that for optimal results some tuning of these parameters could be required. As an example, the 30 km/hr to yield to passenger (Table I) patch has 143 bits and 95.4% digital survivability. Changing s_{lo} to 0.5 results in a smaller 114-pixel perturbation with 94% survivability. This is not entirely unexpected since this is a joint-optimization problem and multiple solutions will exist depend on the weights assigned to different objectives.

One limitation in our work is that our transforms currently simulate viewpoint changes to 2D objects such as flat traffic signs (see Appendix C for description of our transform models). GRAPHITE’s approach is however agnostic to the transforms model. Fundamentally, we just require access to a set of transforms from which we can sample to estimate survivability. Furthermore, the transforms do not have to be differentiable, because we are in the hard-label setting.

One limitation in hard-label attacks is that the starting point has to be a viable solution. Else, there is a risk of getting stuck in a valley with no viable solutions nearby to allow climbing out of the valley. In an earlier version of GRAPHITE,



(a) McAfee’s manually-crafted attack that caused a Tesla to see a 35 miles/hr sign as 85 miles/hr [34]



(b) GRAPHITE-generated image for making a 30 km/hr sign appear as a 80 km/hr sign. The above result had 64% digital survivability.

Fig. 8: An attack discovered by McAfee researchers manually and a similar attack discovered by GRAPHITE automatically

we did not have an automatic mask generation algorithm and were crafting candidate masks by hand. We often ran into situations where patches based on our hand-crafted mask had zero survivability and failed to successfully boost. We found that GRAPHITE significantly alleviates this problem since it starts with a large patch, which is usually survivable, and then reduces and boosts it.

We were curious if GRAPHITE could have been useful in finding a recent widely-reported attack by McAfee researchers [34] that caused a 35 speed limit sign to appear to be a 85 speed limit sign to a Tesla. The attack involved placing black tapes on the 35 speed limit sign (see Figure 8a). Since we were working with the GTSRB dataset that does not contain US signs, we decided to try an attack from 30 km/hr to 80 km/hr sign. GRAPHITE discovered a similar attack using GRAPHITE by tuning the objective function $h(M)$ to favor smaller masks during the fine-grained reduce as long as survivability remained positive (see Fig. 8b). Arguably, the attacks could confuse a human as well, but an auto company researcher has mentioned to us that testing against such attacks is of concern to them.

Finally, we note that we used the number of transforms n to be 100 in our experiments. Using smaller values of n allow adversarial attacks to be generated faster, but the examples may have poorer survivability under a larger number of transforms. For instance, for the stop sign to 30 km/hr attack, for $n = 5$, GRAPHITE generated adversarial examples with 65 pixels but only 54% digital survivability with only 7115 queries. This compares with 123.7k queries and 90% digital survivability for $n = 100$ for the same hyper-parameters. OPT required 33,396 queries for generating the digital-only attack in Fig. 2c. We thus consider GRAPHITE to be relatively query-efficient considering that queries in GRAPHITE also require estimating survivability over multiple samples.

In principle, since GRAPHITE is automated, it can be used as part of an adversarial defense pipeline. However, the algorithm can take a few minutes to produce an attack image. To achieve speedups, a white-box version of GRAPHITE and speeding up heatmap generation would be useful. Determining if a significantly smaller number of transforms suffice in

generating robust attacks and defenses would be a useful future research direction as well.

VIII. RELATED WORK

Physical attacks on computer vision. All existing work for robust physical perturbation attacks on computer vision are in the white-box setting. Examples include printing images of perturbed objects [35], modifying objects with stickers [15], [16], and 3D printing perturbed objects [14]. But, all these methods rely on the availability of gradients from a white-box model to find perturbations that have high survivability under a range of physical transforms such as change of viewing angle, distance, and lighting. To the best of our knowledge, our work is the first to demonstrate robust and query-efficient physical attacks using only top-1 hard-label information.

Furthermore, GRAPHITE, as far as we are aware, is the first to provide an automated method to both generate a small mask and find a robust adversarial example over transforms. Eykholt et al. [15] came closest to that in whitebox settings, suggesting possible ways to identify sensitive areas in an image, but in the end, did not provide an automated method to generate a good mask.

Our work take inspiration from transformation techniques in [15]. We express physical transformations using classical computer vision techniques. For example, we model all geometric transformations (e.g., translation, rotation) using a homography matrix and model lighting changes with a radiometric transformation (see Appendix C).

Digital black-box attacks. There are several categories of digital black-box attacks:

- **Substitute nets:** These *transferability* techniques train a surrogate model, generate white-box examples on the surrogate, and hope they transfer to the target [36]. Unfortunately, targeted example success rates are low [37]. Additionally, these techniques require access to multiple similar training sets that may not be available. By contrast, our work only requires query access to the target model.
- **Gradient estimation:** These *score-based* techniques require access to the softmax layer output in addition to class labels [21], [22]. Using this information, they can apply zeroth order optimization or local search strategies to compute the adversarial example. By contrast, our threat model only allows the attacker top-1 predicted class label access. We construct a gradient-free optimization objective that can create robust examples using only hard-label access.
- **Decision attacks:** A recent line of work has started exploring hard-label attacks in the digital setting [18], [19], [20], [23]. Unfortunately, directly applying physical attack principles from digital settings does not efficiently yield robust adversarial examples that can be used to modify real-world objects (see Section II-F) because the optimization objective is different. For instance, the perturbation magnitude of pixels in digital examples should

be low because the perturbation is added to the entire image and attacks are designed to be imperceptible. By contrast, physical perturbation attacks are less concerned with magnitude and imperceptibility because a perturbation is added to a small region and not the entire object and relies on humans ignoring them. Additionally, decision-based attacks focus on minimizing decision boundary distance and thus attempt to estimate this accurately using queries to the target model. By contrast, physical attacks require survivability against a range of environmental conditions, resulting in changes to the optimization goals. Our work relies on the unique properties of physical adversarial examples, and shows how we can adapt gradient-free optimization to obtain a query-efficient and robust attack.

Black-box physical attacks on audio. There is recent work in the audio domain, and specifically automatic speech recognition (ASR) systems, that uses the threat model of black-box physical attacks [38], [39], [40]. One such approach is based on mangling voice commands based on reverse engineering MFCC features [38], [39], which is specific to the ASR domain. Other approaches build upon the transferability principle [40], where the attacker trains a surrogate model, performs white-box attacks on that model, and then hopes that the attacks transfer to the target. As discussed earlier, our approach does not require a dataset or training a surrogate model; furthermore, adversarial examples based on transferability do not always transfer to the target model, especially when conducting targeted attacks [21], [22]. In contrast, our work is robust on targeted examples and requires only the model’s top-1 predicted label without needing to train a surrogate model. Additionally, robust physical audio adversarial examples with low sound distortion appear to still be an open challenge in the white-box setting [41]. By contrast, our work builds a structured approach in the more established area of vision adversarial examples where white-box attacks are already physically robust [14], [15], [17] and adapt to the black-box setting.

IX. CONCLUSION

We developed GRAPHITE, first automatic algorithm that can create candidates for robust physical perturbation attacks with small masks. GRAPHITE is designed for hard-label black-box setting where adversary has only access to top-1 labels from querying a model. We present a formulation of the objective as a joint optimization problem that aims to find small masks and robust perturbations within those masks. We discuss why the problem is computationally difficult to solve and then present a two-stage optimization process. We present algorithms to first generate masks and then optimize the perturbations for survivability. We show that GRAPHITE produces robust results that can be physically realized: attacking a physical stop sign with stickers generated by GRAPHITE causes a high-accuracy model to output speed limit 30 km/hr in 92.86% of lab tests with high confidence.

ACKNOWLEDGEMENT

This material is based on work supported by DARPA under agreement number 885000, Air Force Grant FA9550-18-1-0166, the National Science Foundation (NSF) Grants 1646392, CCF-FMitF-1836978, SaTC-Frontiers-1804648 and CCF-1652140, and ARO grant number W911NF-17-1-0405. Earlene Fernandes is supported by the University of Wisconsin-Madison Office of the Vice Chancellor for Research and Graduate Education with funding from the Wisconsin Alumni Research Foundation. The U.S. Government is authorized to reproduce and distribute reprints for Governmental purposes notwithstanding any copyright notation thereon. Any opinions, findings, and conclusions or recommendations expressed in this material are those of the author(s) and do not necessarily reflect the views of our research sponsors.

REFERENCES

- [1] F. Schroff, D. Kalenichenko, and J. Philbin, "Facenet: A unified embedding for face recognition and clustering," in *Proceedings of the IEEE conference on computer vision and pattern recognition*, 2015, pp. 815–823.
- [2] A. Krizhevsky, I. Sutskever, and G. E. Hinton, "Imagenet classification with deep convolutional neural networks," in *Advances in neural information processing systems*, 2012, pp. 1097–1105.
- [3] K. Simonyan and A. Zisserman, "Very deep convolutional networks for large-scale image recognition," *arXiv preprint arXiv:1409.1556*, 2014.
- [4] K. He, X. Zhang, S. Ren, and J. Sun, "Deep residual learning for image recognition," in *Proceedings of the IEEE conference on computer vision and pattern recognition*, 2016, pp. 770–778.
- [5] C. Szegedy, V. Vanhoucke, S. Ioffe, J. Shlens, and Z. Wojna, "Rethinking the inception architecture for computer vision," in *Proceedings of the IEEE conference on computer vision and pattern recognition*, 2016, pp. 2818–2826.
- [6] C. Szegedy, W. Zaremba, I. Sutskever, J. Bruna, D. Erhan, I. Goodfellow, and R. Fergus, "Intriguing properties of neural networks," *arXiv preprint arXiv:1312.6199*, 2013.
- [7] I. J. Goodfellow, J. Shlens, and C. Szegedy, "Explaining and harnessing adversarial examples," *arXiv preprint arXiv:1412.6572*, 2014.
- [8] N. Papernot, P. McDaniel, S. Jha, M. Fredrikson, Z. B. Celik, and A. Swami, "The limitations of deep learning in adversarial settings," in *2016 IEEE European symposium on security and privacy (EuroS&P)*. IEEE, 2016, pp. 372–387.
- [9] N. Carlini and D. Wagner, "Towards evaluating the robustness of neural networks," in *2017 IEEE symposium on security and privacy (SP)*. IEEE, 2017, pp. 39–57.
- [10] A. Shafahi, W. R. Huang, M. Najibi, O. Suciu, C. Studer, T. Dumitras, and T. Goldstein, "Poison frogs! targeted clean-label poisoning attacks on neural networks," in *Advances in Neural Information Processing Systems*, 2018, pp. 6103–6113.
- [11] X. Chen, C. Liu, B. Li, K. Lu, and D. Song, "Targeted backdoor attacks on deep learning systems using data poisoning," *arXiv preprint arXiv:1712.05526*, 2017.
- [12] Z. Kolter and A. Madry, "Adversarial Robustness - Theory and Practice," <https://adversarial-ml-tutorial.org/>.
- [13] T. B. Brown, D. Mané, A. Roy, M. Abadi, and J. Gilmer, "Adversarial patch," *arXiv preprint arXiv:1712.09665*, 2017.
- [14] A. Athalye, L. Engstrom, A. Ilyas, and K. Kwok, "Synthesizing robust adversarial examples," *arXiv preprint arXiv:1707.07397*, 2017.
- [15] K. Eykholt, I. Evtimov, E. Fernandes, B. Li, A. Rahmati, C. Xiao, A. Prakash, T. Kohno, and D. Song, "Robust Physical-World Attacks on Deep Learning Visual Classification," in *Computer Vision and Pattern Recognition (CVPR)*, June 2018.
- [16] M. Sharif, S. Bhagavatula, L. Bauer, and M. K. Reiter, "Accessorize to a crime: Real and stealthy attacks on state-of-the-art face recognition," in *Proceedings of the 2016 ACM SIGSAC Conference on Computer and Communications Security*, ser. CCS '16, 2016, p. 1528–1540.
- [17] K. Eykholt, I. Evtimov, E. Fernandes, B. Li, A. Rahmati, F. Tramèr, A. Prakash, T. Kohno, and D. Song, "Physical adversarial examples for object detectors," in *Proceedings of the 12th USENIX Conference on Offensive Technologies*, ser. WOOT'18, 2018.
- [18] M. Cheng, T. Le, P.-Y. Chen, J. Yi, H. Zhang, and C.-J. Hsieh, "Query-efficient hard-label black-box attack: An optimization-based approach," in *International Conference on Learning Representations*, 2019.
- [19] J. Chen, M. I. Jordan, and M. J. Wainwright, "Hopskipjumpattack: A query-efficient decision-based attack," *arXiv preprint arXiv:1904.02144*, 2019.
- [20] A. Ilyas, L. Engstrom, A. Athalye, and J. Lin, "Black-box adversarial attacks with limited queries and information," in *Proceedings of the 35th International Conference on Machine Learning*, 2018, pp. 2137–2146.
- [21] P.-Y. Chen, H. Zhang, Y. Sharma, J. Yi, and C.-J. Hsieh, "Zoo: Zeroth order optimization based black-box attacks to deep neural networks without training substitute models," in *Proceedings of the 10th ACM Workshop on Artificial Intelligence and Security*. ACM, 2017, pp. 15–26.
- [22] N. Narodytska and S. Kasiviswanathan, "Simple black-box adversarial attacks on deep neural networks," in *2017 IEEE Conference on Computer Vision and Pattern Recognition Workshops (CVPRW)*, July 2017, pp. 1310–1318.
- [23] M. Cheng, S. Singh, P.-Y. Chen, S. Liu, and C.-J. Hsieh, "Sign-opt: A query-efficient hard-label adversarial attack," *arXiv preprint arXiv:1909.10773*, 2019.
- [24] Y. Nesterov and V. Spokoiny, "Random gradient-free minimization of convex functions," *Foundations of Computational Mathematics*, vol. 17, no. 2, pp. 527–566, 2017.
- [25] S. Ghadimi and G. Lan, "Stochastic first-and zeroth-order methods for nonconvex stochastic programming," *SIAM Journal on Optimization*, vol. 23, no. 4, pp. 2341–2368, 2013.
- [26] Y. Luo, X. Boix, G. Roig, T. A. Poggio, and Q. Zhao, "Foveation-based mechanisms alleviate adversarial examples," *CoRR*, vol. abs/1511.06292, 2015. [Online]. Available: <http://arxiv.org/abs/1511.06292>
- [27] J. Lu, H. Sibai, E. Fabry, and D. A. Forsyth, "NO need to worry about adversarial examples in object detection in autonomous vehicles," *CoRR*, vol. abs/1707.03501, 2017. [Online]. Available: <http://arxiv.org/abs/1707.03501>
- [28] J. Stallkamp, M. Schlipsing, J. Salmen, and C. Igel, "Man vs. computer: Benchmarking machine learning algorithms for traffic sign recognition," *Neural networks*, vol. 32, pp. 323–332, 2012.
- [29] V. Yadav, "p2-traffic signs," <https://github.com/vxy10/p2-TrafficSigns>, 2016.
- [30] A. Mogelmose, M. M. Trivedi, and T. B. Moeslund, "Vision-based traffic sign detection and analysis for intelligent driver assistance systems: Perspectives and survey," *IEEE Transactions on Intelligent Transportation Systems*, vol. 13, no. 4, pp. 1484–1497, 2012.
- [31] O. Ronneberger, P. Fischer, and T. Brox, "U-net: Convolutional networks for biomedical image segmentation," in *International Conference on Medical image computing and computer-assisted intervention*. Springer, 2015, pp. 234–241.
- [32] J. Redmon and A. Farhadi, "Yolov3: An incremental improvement," *arXiv preprint arXiv:1804.02767*, 2018.
- [33] T.-Y. Lin, M. Maire, S. Belongie, J. Hays, P. Perona, D. Ramanan, P. Dollár, and C. L. Zitnick, "Microsoft coco: Common objects in context," in *European conference on computer vision*. Springer, 2014, pp. 740–755.
- [34] S. Povolny and S. Trivedi, "Model hacking ADAS to pave safer roads for autonomous vehicles," McAfee Labs, Feb. 19, 2020. [Online]. Available: <https://www.mcafee.com/blogs/other-blogs/mcafee-labs/model-hacking-adas-to-pave-safer-roads-for-autonomous-vehicles/>
- [35] A. Kurakin, I. Goodfellow, and S. Bengio, "Adversarial examples in the physical world," *arXiv preprint arXiv:1607.02533*, 2016.
- [36] N. Papernot, P. McDaniel, and I. Goodfellow, "Transferability in machine learning: from phenomena to black-box attacks using adversarial samples," *arXiv preprint arXiv:1605.07277*, 2016.
- [37] Y. Liu, X. Chen, C. Liu, and D. Song, "Delving into transferable adversarial examples and black-box attacks," *CoRR*, vol. abs/1611.02770, 2016. [Online]. Available: <http://arxiv.org/abs/1611.02770>
- [38] N. Carlini, P. Mishra, T. Vaidya, Y. Zhang, M. Sherr, C. Shields, D. Wagner, and W. Zhou, "Hidden voice commands," in *25th {USENIX} Security Symposium ({USENIX} Security 16)*, 2016, pp. 513–530.
- [39] T. Vaidya, Y. Zhang, M. Sherr, and C. Shields, "Cocaine noodles: exploiting the gap between human and machine speech recognition,"

in 9th {USENIX} Workshop on Offensive Technologies ({WOOT} 15), 2015.

- [40] Y. Chen, X. Yuan, J. Zhang, Y. Zhao, K. Zhang, Shengzhi Chen, and X. Wang, “Devil’s whisper: A general approach for physical adversarial attacks against commercial black-box speech recognition devices,” in *29th USENIX Security Symposium (USENIX Security 20)*, 2020.
- [41] Y. Qin, N. Carlini, G. Cottrell, I. Goodfellow, and C. Raffel, “Imperceptible, robust, and targeted adversarial examples for automatic speech recognition,” in *Proceedings of the 36th International Conference on Machine Learning*, ser. Proceedings of Machine Learning Research, vol. 97. Long Beach, California, USA: PMLR, 09–15 Jun 2019, pp. 5231–5240. [Online]. Available: <http://proceedings.mlr.press/v97/qin19a.html>
- [42] S. Boucheron, G. Lugosi, and P. Massart, *Concentration Inequalities*. Oxford University Press, 2013.

APPENDIX A

NP-COMPLETENESS OF MASK GENERATION

A $n \times n$ square grid is represented as G_n , which is a graph (V_n, E_n) (V_n has vertices (i, j) , where $0 \leq i \leq n$ and $0 \leq j \leq n$ and for each (i, j) , $\{(i, j+1), (i, j-1), (i+1, j), (i-1, j)\} \cap V_n$ is in the set of edges E_n). A mask M is a sub-graph of the grid G_n that corresponds to a contiguous region of squares. Let $C(G_n)$ be the set of masks corresponding to the grid G_n . Let $\mu : C(G_n) \rightarrow \mathbb{R}^+$ be a *monotonic scoring function* ($M \subseteq M'$ implies that $\mu(M) \leq \mu(M')$). The mask generation problem can be stated as follows: Given r and threshold t , find a mask M of size $\leq r$ (the size of the mask is number of squares in it) such that $\mu(M) \geq t$. We call this problem $\text{MASK}_P(n, \mu, r, t)$.

Simply enumerating masks is not feasible because the number of masks could be exponential. We provide a simple argument. Consider a $k \times k$ sub-grid of G_n . Consider columns that are odd numbered (i.e. of the form (i, \star) , where i is odd). Now any choice of one square for the even columns gives us a contiguous mask, so there are $\geq 2^{\frac{k(k+1)}{2}}$ masks. There are $(n-k)^2$ $k \times k$ sub-grids in G_n . So a lower bound on masks of size k is at least $(n-k)^2 2^{\frac{k(k+1)}{2}}$. Next we prove that our problem is actually NP-complete.

The Set Cover. Given a universe \mathcal{U} and a family \mathcal{S} of subsets of \mathcal{U} , a cover is a subfamily $\mathcal{C} \subseteq \mathcal{P}(\mathcal{U})$ of sets whose union is \mathcal{U} . In the set-covering decision problem, the input is a triple $(\mathcal{U}, \mathcal{S}, k)$ (k is an integer), and the question is *whether there is a set covering of size k or less*. In the set covering optimization problem, the input is a pair $(\mathcal{U}, \mathcal{S})$ and the task is to find a set covering that uses the fewest sets. The set-covering decision problem is known to be NP-complete.

Theorem 1: Problem MASK_P is NP-complete.

Proof. Our reduction will be from the decision set-cover problem. Assume we are given an instance of the set-cover problem $(\mathcal{U}, \mathcal{S}, k)$. Let $n = \max(|\mathcal{U}|, |\mathcal{S}|)$. We create a $n \times n$ grid G_n . Let $C(G_n)$ be the set of masks of G_n . We construct a scoring function μ as follows: Let M be a mask. Let $I = \{i | (i, 0) \in M\}$, and $\mathcal{S}_I = \{S_j | j \in I \wedge S_j \in \mathcal{S}\}$. $\mu(M) = 1$ if and only if the following condition holds (otherwise $\mu(M) = 0$): $|I| \leq k$ and $\cup_{j \in I} S_j = \mathcal{U}$. It is easy to see that $\text{MASK}_P(n, \mu, n^2, 1)$ has a satisfying solution iff the instance of the set cover problem has a solution. This proves that the problem is NP-hard. Given a solution to the problem $\text{MASK}_P(n, \mu, r, t)$, it is easy to check that it is a valid

solution in polynomial time, so the problem is NP. Therefore, $\text{MASK}_P(n, \mu, r, t)$ is NP-complete. \square

APPENDIX B

SAMPLING ERROR

There are several versions of Chernoff’s bounds [42]. We state in Theorem 1 a form that is most convenient for us.

Theorem 1:

Let X_1, \dots, X_n be iid binary variables such that $P(X_i = 1) = p$ (thus $P(X_i = 0) = 1 - p$), and let $A = \sum_{i=1}^n X_i$. In this case, we have the following inequality:

$$P(|\frac{A}{n} - p| \geq \zeta p) \leq 2e^{-\frac{n p \zeta^2}{3}} \quad (15)$$

Consider the probability inside (10), which we denote as q . Let us sample n transformations $\{t_1, \dots, t_n\}$ from distribution T . Let X_i be equal to 1 if $F(t(x + M \cdot \delta)) \neq y_{adv}$, and 0 otherwise. By definition $P(X_i = 1)$ is equal to q . By Theorem 1 we have that (we instantiate the theorem with $\epsilon = \zeta q$ and $A = \sum_{i=1}^n X_i$), where ϵ represents the error in our solution due to sampling.

$$P(|\frac{A}{n} - q| \geq \epsilon) \leq 2e^{-\frac{n q \epsilon^2}{3\epsilon^2}} \quad (16)$$

Or in other words

$$P(|\frac{A}{n} - q| < \epsilon) \geq 1 - 2e^{-\frac{n q \epsilon^2}{3\epsilon^2}} \quad (17)$$

APPENDIX C

MODELING PHYSICAL TRANSFORMS USING CLASSICAL COMPUTER VISION

Prior work by Eykholt et al. [15] and Athalye et al. [14] model environmental effects to create physical-world attacks in the white-box setting. These transformations account for varying conditions such as the distance and angle of the camera, lighting conditions, etc. Based on this work, we build a more principled set of transformations using classical computer vision techniques. To this end, we group these effects into 3 main classes of transformations:

- 1) **Geometric transformations:** These transformations refer to shape-based changes including rotation, translation and zoom. For planar objects, all three effects can be captured in a single perspective transformation through a homography matrix. Homography matrices relate two planar views under different perspectives. Geometrically, to convert points from one image plane to another, one can break down the operation into a rotation and translation matrix R , perspective projection onto a plane (P), and an affine transformation from plane to pixels (A). In the planar case, this boils down to a 3×3 homography matrix H :

$$x_{out} = APRx_{in} = Hx_{in} \quad (18)$$

We use these homographies to simulate rotation around the y axis and different viewing distances for given

ranges of values. Once we pick values for each of the parameters uniformly, we construct the homography matrix to compute the transformation.

After performing the perspective transform, we random crop to the tightest square crop that includes the whole object $\pm c\%$ of the resultant image size to adjust for cropping errors. We also add random offsets for the crop, given as two more parameters. Then, we resize the square to the original resolution.

- 2) **Radiometric transformations:** These are appearance-based transformations with effects such as lighting-based changes. One technique to perform brightness adjustments is gamma correction, which applies a nonlinear function. Separately, printers apply nonlinear functions to their colorspace as well. Gamma correction is reflective of nonlinear human sight perception. To model these radiometric-based changes, we model gamma correction under gamma values between $\frac{1}{\gamma}$ and γ , with half coming from $[\frac{1}{\gamma}, 1]$ and half coming from $[1, \gamma]$ in expectation where γ is the maximum gamma value allowed. Assuming the image ranges from $[0, 1]$, this is defined as the following:

$$x_{out} = x_{in}^{\gamma} \quad (19)$$

- 3) **Filtering transformations:** These transformations model changes related to the camera focus. We model Gaussian blurring of different kernel sizes to measure the effects of the target object being out-of-focus. We note that as a side benefit, this may help deal with printer error as some precision in color values is lost in printing.

We define a single transformation to be a composite function that includes one of each type of modeled transformation. In our case with those listed above, we would have a perspective transform followed by a cropping operation, gamma correction, and a Gaussian blur convolution. Examples of transformed images are shown in Figure 9.

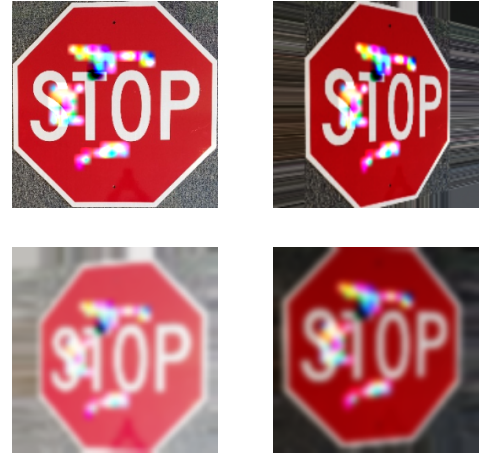


Fig. 9: Examples of different transformed images. The upper-left image is the original, and the rest are three examples of transformed versions with perspective, lighting, and blurring transforms.